G. Quaranta, A. Tamer, V. Muscarello, P. Masarati, M. Gennaretti, J. Serafini, M. Molica Colella
Rotorcraft Aeroelastic Stability Using Robust Analysis
CEAS Aeronautical Journal, Vol. 5, N. 1, 2014, p. 29-39
doi:10.1007/s13272-013-0082-z

Noname manuscript No.
(will be inserted by the editor)

ROTORCRAFT AEROELASTIC STABILITY USING ROBUST ANALYSIS

Giuseppe Quaranta · Aykut Tamer · Vincenzo Muscarello · Pierangelo Masarati
Massimo Gennaretti · Jacopo Serafini · Marco Molica Colella

Received: date / Accepted: date

Abstract

This paper discusses the impact of different models of aerodynamic loads on rotorcraft-pilot couplings stability using a robust stability analysis approach. The aeroelasticity of the main rotor of a helicopter is formulated using aerodynamic models based on blade element/momentum theory and boundary element method coupled to a finite element model of the blade. The resulting linearized models are used to determine stability limits according to the generalized Nyquist criterion, associated with the accelerations of the pilot's seat caused by the involuntary action of the pilot on the control inceptors. The resulting stability curves are discussed considering examples of involuntary pilot transfer functions from the literature.

Keywords Rotorcraft Aeroelasticity · Robust Stability · Rotorcraft-Pilot Couplings

1 Introduction

Robust stability analysis techniques enable the evaluation of the stability margins of systems with respect to uncertain parameters [1,2]. Their application to rather heterogeneous aspects of system dynamics is the result of their generality and versatility [3–7]. Many aspects of rotorcraft aeroservoelasticity may benefit from robust stability analysis, especially when intrinsically uncertain aspects of the model must be addressed; for example, the constitutive properties of lead-lag dampers in the study of ground resonance [8, 9], or the involuntary dynamics of the pilot in the study of Rotorcraft-Pilot Couplings (RPC) [10, 11].

Giuseppe Quaranta · Aykut Tamer
Vincenzo Muscarello · Pierangelo Masarati
Dipartimento di Scienze e Tecnologie Aerospaziali, Politecnico di Milano, Via La Masa 34 20156 Milano - Italy
Tel.: +39 02 23998405
Fax: +39 02 23998334
E-mail: giuseppe.quaranta@polimi.it

Massimo Gennaretti · Jacopo Serafini · Marco Molica Colella
Dipartimento di Ingegneria, Università Roma Tre, via della Vasca Navale 79 00146 Roma - Italy

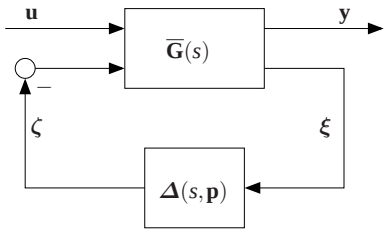

Fig. 1 Feedback loop between nominal plant $\overline{\mathbf{G}}(s)$ and uncertainty operator $\Delta(s,\mathbf{p})$.

The theory stems from the consideration that by writing the dynamics of a stable system in the form of a feedback loop, as shown in Figure 1, where the uncertainty $\Delta(s,\mathbf{p})$ is concentrated in the feedback path of the loop, the stability of the closed loop system can be analyzed by simply looking at the eigenlocus of the loop transfer function, according to the Generalized Nyquist Criterion (GNC). This, in turn is written as a multiplicative function of a portion of the part of the system that is considered certain, $\mathbf{G}(s)$, by the part that is considered uncertain, $\Delta(s,\mathbf{p})$, namely $\mathbf{H}(s) = \Delta(s,\mathbf{p})\mathbf{G}(s)$.

When any of the eigenvalues of the loop transfer matrix $\mathbf{H}(\mathrm{j}\omega)$ reaches the point $(-1+\mathrm{j}0)$ in the Argand plane (the complex plane), the system becomes unstable. The distance of the eigenvalues of the nominal plant from the point $(-1+\mathrm{j}0)$ represents a powerful, yet intuitive measure of the stability margin of the system, which is defined for each frequency.

The aerodynamic forces acting on the rotor may represent a significant source of uncertainty, owing to local three-dimensional and compressibility effects, Blade-Vortex Interaction (BVI), and so on. When the aeroservoelasticity of the

overall vehicle is of concern, often using Ritz-like reduced order models to describe the structural dynamics of the system, the generalized unsteady aerodynamic loads may be computed from relatively sophisticated, yet uncertain models. As long as the source of the uncertainty can be somehow identified, e.g. in the form of amplitude and phase of the transfer functions relating the airframe motion to the loads transmitted by the rotor to the airframe, appropriate margins with respect to the stability of the overall aeroservoelastic system can be determined.

In detail, the proposed approach makes it possible to determine how sensitive the stability of the system is with respect to uncertainties in the modeling of the main rotor aeroelasticity (with particular attention to the aerodynamic contribution). In fact, significant sensitivity would indicate that a refinement and an improvement of the quality of the modeling is mandatory. Otherwise, as long as the impact of the uncertainty is minimal, relatively inaccurate models could be tolerated, being the quality of the aeroelastic (aerodynamic) modeling not essential for the purpose of the analysis.

This work originates from the need to analyze Rotorcraft-Pilot Couplings (RPC) within the research project ARISTOTEL[1], partially supported by the European Commission within the 7th Framework Programme. The possibility to limit the complexity of the analysis of critical components of the aeroservoelastic system is in fact of paramount importance to reduce the computational cost and to make it possible to focus on essential aspects of the problem.

The robust stability analysis requires to act on Linear Time Invariant (LTI) models of the plant. In the present analysis, the aeroservoelasticity of the helicopter is modeled in the MASST environment, developed at Politecnico di Milano [12, 13]. The aeroelastic LTI model of the main rotor is developed by the University 'Roma Tre', starting from validated computational tools for rotor aeroelastic response analysis [14] and subsequently applying the methodology presented in Ref. [15] for identification and finite-state modeling of the aerodynamic operator regarding rotors in arbitrary steady flight. This approach requires the prediction of a set of harmonic perturbation responses by an aeroelastic solver, and the accuracy of the identified model in describing the unsteady loads transmitted by the rotor to the airframe is strictly connected to that of the aerodynamic solver applied within the aeroelastic tool.

The proposed approach is applied to a rotorcraft model jointly developed by Politecnico di Milano and University 'Roma Tre' within the project ARISTOTEL. Applying two independent quasi-steady sectional aerodynamic formulations and a Boundary Element Method (BEM) potential-flow solution within the aeroelastic solver [14], stability boundaries are computed in the space of the pilot biodynamic feedthrough functions, which represent the formally uncertain feedback operator in the analysis. The stability boundaries resulting from the different aerodynamic models are compared, to understand how sensitive they are to the complexity level in aerodynamics modeling. In fact, both the involuntary behavior of the pilot and the aeromechanics of the vehicle present some degree of uncertainty; however, the uncertainty of the pilot's behavior is intrinsic, as different subjects may behave differently even in similar conditions, and even the same subject may behave differently under different conditions, whereas the uncertainty in the aeromechanical properties of the vehicle is essentially related to the degree of approximation introduced in the numerical models.

[1] http://www.aristotel.progressima.eu/

2 Robust Stability Analysis

Robust stability analysis is based on the assumption that the transfer matrix $\overline{\mathbf{G}}(s)$ between the input vector $\mathbf{u}(s)$ and the output vector $\mathbf{y}(s)$ of a system characterized by a set of uncertain parameters $\mathbf{p}$,

$$\mathbf{y}(s) = \overline{\mathbf{G}}(s,\mathbf{p})\mathbf{u}(s), \tag{1}$$

under broad assumptions can be cast as

$$\begin{Bmatrix} \mathbf{y} \\ \boldsymbol{\eta} \end{Bmatrix} = \begin{bmatrix} \mathbf{G}_{11} & \mathbf{G}_{12} \\ \mathbf{G}_{21} & \mathbf{G}_{22} \end{bmatrix} \begin{Bmatrix} \mathbf{u} \\ \boldsymbol{\zeta} \end{Bmatrix} \tag{2}$$

using a Linear Fractional Transform (LFT) [16], where a negative feedback loop can be established on the transfer matrix $\boldsymbol{\Delta}$ of the uncertain part, $\boldsymbol{\zeta} = -\boldsymbol{\Delta}\boldsymbol{\eta}$, yielding

$$\mathbf{y}(s) = \left(\mathbf{G}_{11} - \mathbf{G}_{12}\boldsymbol{\Delta}\left(\mathbf{I} + \mathbf{G}_{22}\boldsymbol{\Delta}\right)^{-1}\mathbf{G}_{21}\right)\mathbf{u}(s), \tag{3}$$

as shown in Fig. 1. The m parameters collected in vector $\mathbf{p}$ are uncertain but bounded; they belong to the set

$$\mathscr{P} = \{\mathbf{p} :\ \mathbf{p} = \mathbf{p}_0 + \delta\mathbf{p},\ \delta\mathbf{p} \subset \mathbb{R}^m\}, \tag{4}$$

where $\mathbf{p}_0$ corresponds to the nominal parameters of the aircraft without uncertainty.

Under the assumption that the baseline system $\overline{\mathbf{G}}$, with $\boldsymbol{\Delta} \equiv \boldsymbol{\Delta}_0$, is stable, and that $\boldsymbol{\Delta}$ itself is stable for all $\mathbf{p} \in \mathscr{P}$, the stability of the uncertain system of Eq. (3) can be studied by considering that of the transfer matrix

$$\mathbf{H}(\mathrm{j}\omega) = \mathbf{G}_{22}(\mathrm{j}\omega)\boldsymbol{\Delta}(\mathrm{j}\omega), \tag{5}$$

which plays the role of the loop transfer function in classical feedback control theory [2]. The stability of the transfer matrix of Eq. (5), in turn, can be studied using the GNC by considering the distance of the eigenvalues of the loop transfer matrix $\mathbf{H}(\mathrm{j}\omega)$ from the point $(-1+\mathrm{j}0)$ as a function of the uncertain parameters, whose limit values are found by requiring such distance to vanish, namely $\det(\mathbf{I}+\mathbf{H}(\mathrm{j}\omega)) = 0$.

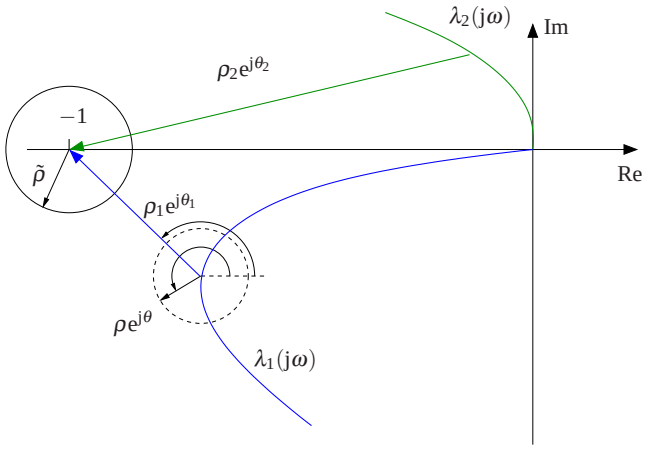

Fig. 2 Nyquist eigenloci: distance of transfer matrix eigenvalues from point $(-1+\mathrm{j}0)$ in the complex plane.

The perturbation of the i-th eigenvalue $\lambda_i(\mathbf{H}_0(\mathrm{j}\omega))$ of the reference system $\mathbf{H}_0 = \mathbf{G}_{22}\boldsymbol{\Delta}_0$ can be expressed as

$$\lambda_i(\mathbf{H}(\mathrm{j}\omega)) = \lambda_i(\mathbf{H}_0(\mathrm{j}\omega)) + \rho e^{\mathrm{j}\theta}, \tag{6}$$

where the complex number $\rho e^{\mathrm{j}\theta}$ represents an arbitrary perturbation of the i-th eigenvalue of modulus ρ and argument θ, as shown in Figure 2.

When $\lambda_i(\mathbf{H}(\mathrm{j}\omega)) = -1$ the stability limit is reached for eigenvalue λ_i, since the loop transfer function corresponding to that eigenvalue for any further perturbation would circle about point $(-1+\mathrm{j}0)$. As a consequence, the stability margin, as a function of the frequency ω, is

$$\rho_i(\omega) e^{\mathrm{j}\theta_i(\omega)} = -(\lambda_i(\mathbf{H}_0(\mathrm{j}\omega)) + 1). \tag{7}$$

For each frequency ω, the critical direction $\theta_i(\omega)$ represents the direction from $\lambda_i(\mathbf{H}_0(\mathrm{j}\omega))$ to $(-1+\mathrm{j}0)$ and $\rho_i(\omega)$ represents the magnitude of the eigenvalue perturbation that leads to instability when it occurs along the critical direction (Fig. 2).

The most critical eigenvalue among those of matrix $\mathbf{H}_0$ is the one whose distance is the smallest among those computed for all eigenvalues. However, depending on the structure of the uncertainty, the sensitivity of the eigenvalues of matrix $\mathbf{H}_0$ to uncertain parameters may determine their actual criticality. The distance of the eigenvalues from the point $(-1+\mathrm{j}0)$ can be transformed into frequency-dependent boundaries for the uncertain parameters using the notion of left, $\mathbf{v}_{Li}$, and right eigenvectors, $\mathbf{v}_{Ri}$, respectively solutions of the eigenvalue problems

$$\mathbf{H}\mathbf{v}_{Ri} = \mathbf{v}_{Ri}\lambda_i \tag{8a}$$

$$\mathbf{H}^T\mathbf{v}_{Li} = \mathbf{v}_{Li}\lambda_i, \tag{8b}$$

with $\mathbf{V}_L^T = \mathbf{V}_R^{-1}$ when all left and right eigenvectors are collected in matrices $\mathbf{V}_L$ and $\mathbf{V}_R$, respectively, since by definition

$$\mathbf{v}_{Li}^T\mathbf{H}\mathbf{v}_{Ri} = \lambda_i. \tag{9}$$

Considering an additive uncertainty $\boldsymbol{\Delta} = \boldsymbol{\Delta}_0 + \delta\boldsymbol{\Delta}$, the left and right eigenvectors of the nominal system can be used to express the critical condition as

$$\begin{aligned}
&\mathbf{v}_{Li}^T\mathbf{H}(\mathrm{j}\omega)\mathbf{v}_{Ri} \\
&= (\mathbf{v}_{0Li} + \delta\mathbf{v}_{Li})^T (\mathbf{H}_0(\mathrm{j}\omega) + \delta\mathbf{H}_{\lim}(\mathrm{j}\omega)) (\mathbf{v}_{0Ri} + \delta\mathbf{v}_{Ri}) \\
&\cong \lambda_{0i} + \mathbf{v}_{0Li}^T\delta\mathbf{H}_{\lim}(\mathrm{j}\omega)\mathbf{v}_{0Ri} = -1,
\end{aligned} \tag{10}$$

where $\delta\mathbf{H} = \mathbf{G}_{22}\delta\boldsymbol{\Delta}$, and $\delta\mathbf{H}_{\lim}$ indicates the perturbation of $\mathbf{H}$ at the verge of stability. Equation (10) expresses a first-order approximation of the eigenvalue change, since the contribution associated with the eigenvector changes $\delta\mathbf{v}_{Li}$ and $\delta\mathbf{v}_{Ri}$ is second-order with respect to $\delta\lambda_i$ according to a generalization of Rayleigh's quotient.

In fact, considering terms in Eq. (10) only up to first-order, one obtains

$$\begin{aligned}
&\mathbf{v}_{Li}^T\mathbf{H}(\mathrm{j}\omega)\mathbf{v}_{Ri} \\
&\cong \mathbf{v}_{0Li}^T\mathbf{H}_0\mathbf{v}_{0Ri} + \mathbf{v}_{0Li}^T\mathbf{H}_0\delta\mathbf{v}_{Ri} + \delta\mathbf{v}_{Li}^T\mathbf{H}_0\mathbf{v}_{0Ri} + \mathbf{v}_{0Li}^T\delta\mathbf{H}\mathbf{v}_{0Ri} \\
&= \lambda_{0i} + \lambda_{0i}\left(\mathbf{v}_{0Li}^T\delta\mathbf{v}_{Ri} + \delta\mathbf{v}_{Li}^T\mathbf{v}_{0Ri}\right) + \mathbf{v}_{0Li}^T\delta\mathbf{H}\mathbf{v}_{0Ri},
\end{aligned} \tag{11}$$

since $\mathbf{v}_{0Li}^T\mathbf{H}_0 = \lambda_{0i}\mathbf{v}_{0Li}^T$ and $\mathbf{H}_0\mathbf{v}_{0Ri} = \mathbf{v}_{0Ri}\lambda_{0i}$. However, since the eigenvectors can be arbitrarily normalized as $\mathbf{v}_{Li}^T\mathbf{v}_{Ri} \equiv 1$, then

$$\mathbf{v}_{Li}^T\mathbf{v}_{Ri} \cong \mathbf{v}_{0Li}^T\mathbf{v}_{0Ri} + \mathbf{v}_{0Li}^T\delta\mathbf{v}_{Ri} + \delta\mathbf{v}_{Li}^T\mathbf{v}_{0Ri} + \delta\mathbf{v}_{Li}^T\delta\mathbf{v}_{Ri}, \tag{12}$$

which yields $\mathbf{v}_{0Li}^T\delta\mathbf{v}_{Ri} + \delta\mathbf{v}_{Li}^T\mathbf{v}_{0Ri} = -\delta\mathbf{v}_{Li}^T\delta\mathbf{v}_{Ri}$; as a consequence, the first-order terms associated to perturbations of the eigenvectors are equivalent to terms that are second-order in the perturbation of the eigenvalues. Note that, from the comparison of Eqs. (6), (9) and (10) it is possible to gather that $\rho e^{\mathrm{j}\theta} \cong \mathbf{v}_{0L}^T\delta\mathbf{H}(\mathrm{j}\omega)\mathbf{v}_{0R}$. According to Eq. (10) one obtains

$$\rho_i(\omega) e^{\mathrm{j}\theta_i(\omega)} \cong -1 - \lambda_{0i} = \mathbf{v}_{0Li}^T\delta\mathbf{H}_{\lim}(\mathrm{j}\omega)\mathbf{v}_{0Ri}. \tag{13}$$

When the parameter change implies a non-negligible change in the eigenvectors, the problem

$$\mathbf{v}_{Li}^T\mathbf{H}_{\lim}(\mathrm{j}\omega)\mathbf{v}_{Ri} = -1, \tag{14}$$

as in Eq. (10) but without any approximation, must be solved to determine the value of the parameter perturbation that takes the system to the verge of stability. An approach based on continuation can be used; its discussion is outside the scope of this work.

When $\rho(\omega) < \min_i(\rho_i(\omega))\ \forall\omega$, stability is granted. Otherwise, it is necessary that $\theta \neq \theta_k$, where k indicates the eigenvalue corresponding to $\min_i(\rho_i)$. This can be stated as

$$\rho(\omega) e^{\mathrm{j}\theta(\omega)} < \rho_k(\omega) e^{\mathrm{j}\theta_k(\omega)}, \qquad k : \rho_k = \min_i(\rho_i(\omega)), \tag{15}$$

where operator $(\cdot) < (\cdot)$ applied to complex numbers compares their moduli when the argument is the same.

Further margins can be considered by requiring the uncertain bounds to allow some residual distance from point $(-1+\mathrm{j}0)$. This can be obtained by first computing the critical direction θ_i that leads from point λ_{0i} to point $(-1+\mathrm{j}0)$, namely

$$d = -\frac{1+\lambda_{0i}}{\|1+\lambda_{0i}\|} = \mathrm{e}^{\mathrm{j}\theta_i}. \tag{16}$$

Then, a new uncertainty amplitude $\hat{\rho}_i$, that leaves a prescribed margin $\tilde{\rho}$ along the critical direction, is considered,

$$\hat{\rho}_i = \rho_i - \tilde{\rho}. \tag{17}$$

This corresponds to considering the distance ρ_i of the i-th eigenvalue from the point $(-1+\mathrm{j}0)$, along the critical direction θ_i, as shown in Figure 2, and restricting the limit value such that, when at the boundary, a residual distance $\tilde{\rho}$ remains.

3 Problem Description

An aeroservoelastic model of a helicopter representative of the Messerschmitt-Bölkow-Blohm (MBB) BO105 has been developed in MASST using the technical data reported in [17, 18]. This helicopters has been selected because it is considered representative of small-size, hingeless helicopters. Its general characteristics are summarized in Table 1.

Table 1 BO105 general characteristics.

Parameter	Value	Units
Gross weight	2055.0	kg
CG station	3318.0	mm
Max. flight speed	140.0	kts
Main rotor radius	4.9	m
Main rotor solidity	7.02	%
Main rotor lock number	4.31	n.d.
Main rotor angular velocity	424.0	rpm
Main rotor flap frequency	1.1	/rev
Main rotor lag frequency	0.68	/rev

3.1 Rotor Aeroelasticity Subproblem

From the point of view of the interaction with the rest of the vehicle, the Main Rotor (MR) contribution is expressed in terms of a LTI aeroelastic operator. For a given steady flight condition, it relates forces and moments produced by the rotor at the MR attachment point, $\mathbf{f}_{\mathrm{MR}}$, to the components of motion at that point (displacements and rotations), $\mathbf{x}_{\mathrm{MR}}$, and to the MR controls, $\boldsymbol{\delta}_{\mathrm{MR}} = \{\theta_0; \theta_{1c}; \theta_{1s}\}$, namely

$$\mathbf{f}_{\mathrm{MR}} = \mathbf{H}_{\mathbf{x}\mathrm{MR}}(\mathrm{j}\omega)\mathbf{x}_{\mathrm{MR}} + \mathbf{H}_{\boldsymbol{\delta}\mathrm{MR}}(\mathrm{j}\omega)\boldsymbol{\delta}_{\mathrm{MR}}. \tag{18}$$

Note that the rotation components of the motion are point functions in that they include both rigid-body motion and deformation effects of the airframe. In practice, these loads are evaluated in the frequency domain for a set of discrete frequencies and for a given set of trim points, ranging from hover to forward flight at different speeds. Variations of the aeroelastic solver applied to sample matrices $\mathbf{H}_{\mathbf{x}\mathrm{MR}}$ and $\mathbf{H}_{\boldsymbol{\delta}\mathrm{MR}}$ enables one to carry out sensitivity analyses of the predicted dynamic behavior of the coupled rotorcraft-pilot system with respect to uncertainties in main rotor aerodynamic (and structural, eventually) modeling.

3.1.1 The Aeroelastic Solver (in brief)

A beam-like model [15] is used to describe the structural dynamics of rotor blades. It is based on the nonlinear bending-torsion formulation presented in Ref. [19], that is valid for straight, slender, homogeneous, isotropic, nonuniform, twisted blades, undergoing moderate displacements. The radial displacement is eliminated from the set of equations by solving it in terms of local tension, and thus the resulting structural operator consists of a set of coupled nonlinear differential equations governing the bending of the elastic axis (lead-lag and flap deflections) and the rotation of the cross-sections (blade torsion). If present, the effects of blade pre-cone angle, hinge offset, torsion offset and mass offset are included in the model, as well as the kinematic effects due to hub motion.

Combining this structural dynamics model with a model describing the distributed aerodynamic loads yields the aeroelastic formulation. In this work, the rotor aerodynamic loads are simulated either through a quasi-steady, sectional model with wake-inflow corrections taking into account the three-dimensional trailing vortices influence (see, for instance, Ref. [14]), or through a BEM solver for free-wake, potential flows. In particular, the BEM computational tool considered is based on the formulation suited for the prediction of BVI effects presented and validated in Refs. [20, 21], and therefore is applicable to a wide range of rotor flight configurations, including descent patterns. The blade pressure distribution, p, is determined using the Bernoulli theorem and the distributed forces and torsional moment are obtained by integration over cross-section profile contours.

The resulting aeroelastic integro-differential formulation is integrated spatially using the Galerkin approach, and the time response is computed through a time marching, Newmark-β numerical scheme.

Once the aeroelastic response is computed, forces and moments at the MR attachment point are evaluated by integration of the corresponding aerodynamic and inertial loads arising along the span of the blades.

3.1.2 Sampling of the LTI Aeroelastic Operator

For a helicopter rotor in arbitrary steady flight, the aeroelastic model described above is intrinsically nonlinear, with periodic coefficients. As a consequence, even a single-harmonic, small perturbation of MR controls or hub motion yields multiharmonic loads at the MR attachment point (and thus, cannot be modeled through a LTI operator). However, as widely applied in aeroelastic, multiblade-variable analyses of isolated helicopter rotors, for the objectives of the present problem accurate linearized modeling can be based on the time-invariant approximation (indeed, it involves I/O quantities defined in the nonrotating frame).

Following the approach presented in Ref. [15] regarding the LTI modeling of the aerodynamic loads of rotors in arbitrary steady flight, in this work the MR LTI aeroelastic model is obtained from the complete aeroelastic solution in the way herein described:

(i) the time marching aeroelastic solver is used to evaluate the perturbation loads at the MR attachment point due to single-harmonic small oscillations of each variable in $\mathbf{x}_{\mathrm{MR}}$ and $\boldsymbol{\delta}_{\mathrm{MR}}$;
(ii) the response harmonic component having the same frequency of the input is extracted;
(iii) the corresponding complex values of the frequency-response function are determined;
(iv) the process is repeated for a discrete number of frequencies within an appropriate range, so as to get an adequate sampling of the frequency-response functions appearing within $\mathbf{H}_{\mathbf{x}\mathrm{MR}}$ and $\mathbf{H}_{\boldsymbol{\delta}\mathrm{MR}}$.

In other words, the procedure applied is such that only the constant-coefficient, linear(ized), portions of the operator relating perturbations of $\mathbf{x}_{\mathrm{MR}}$ and $\boldsymbol{\delta}_{\mathrm{MR}}$ to $\mathbf{f}_{\mathrm{MR}}$ are retained [15].

It is worth mentioning that the harmonic components are obtained through a Fast Fourier Transform (FFT) algorithm, taking care of the following issues:

(i) the period examined by the FFT starts after that the aeroelastic transient response to the perturbation is finished;
(ii) the period examined has to be an integer multiple of the period of the input harmonic;
(iii) almost periodic loads might arise because of the intrinsic periodicity of the aeroelastic system, and hence the leakage avoidance is assured if, in addition, the examined period is long enough.

Finally, note that the described approach can only be applied if the isolated rotor is asymptotically stable for the steady flight configuration about which the LTI model is identified.

The transfer functions identified through the aeroelastic solver based on Blade Element theory and those obtained using aeroelastic predictions derived from the application of the BEM solver are compared in Figs. 3 and 4. Figure 3 contains the thrust component of the rotor force as a function of the axial motion of the hub, while Fig. 4 contains the roll moment as a function of the lateral cyclic pitch control. In both cases, the two solutions show a similar trend with respect to frequency. This is expected, since rotor blade elastic properties have a strong influence on poles and zeroes of the aeroelastic response function. However, some discrepancies arise, which imply non-negligible local differences in amplitude and phase of the response.

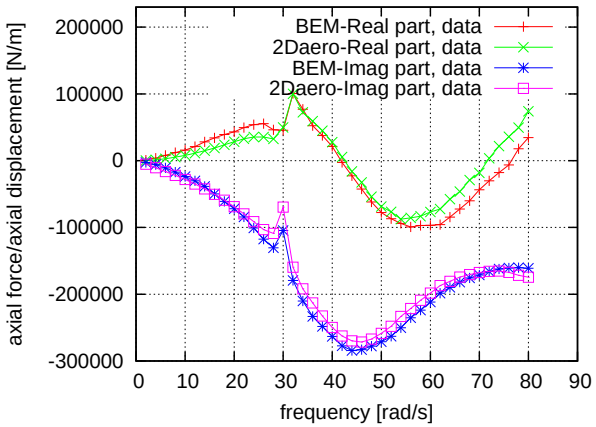

Fig. 3 MR vertical force vs. axial hub motion.

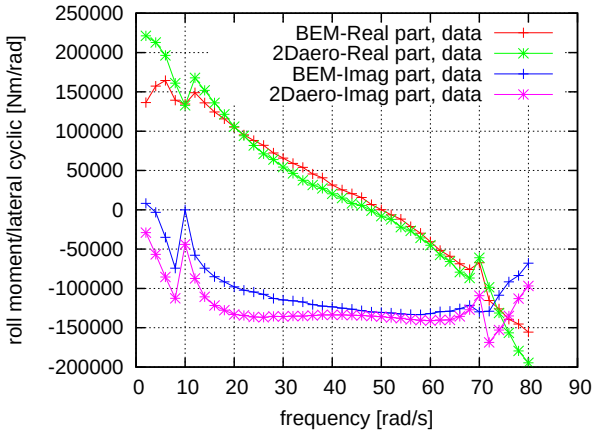

Fig. 4 MR roll moment vs. lateral cyclic pitch.

3.2 Airframe Dynamics Problem

The structural dynamics model simply consists of the second-order equations of the rigid-body and flexible airframe dynamics,

$$\mathbf{M}\ddot{\mathbf{q}} + \mathbf{C}\dot{\mathbf{q}} + \mathbf{K}\mathbf{q} = \mathbf{f}, \tag{19}$$

formulated for the modal variables $\mathbf{q}$. The motion of the MR attachment point is known in terms of the corresponding modal displacements $\mathbf{x}_{\mathrm{MR}} = \mathbf{U}_{\mathrm{MR}}\mathbf{q}$. As a consequence,

the frequency domain representation of the airframe dynamics is simply coupled to the MR aeroelastic model using the Principle of Virtual Work (PVW), namely

$$\begin{aligned}\delta\mathscr{W}_{\mathrm{MR}} &= \delta\mathbf{x}_{\mathrm{MR}}^T\mathbf{f}_{\mathrm{MR}} \\ &= \delta\mathbf{q}^T\mathbf{U}_{\mathrm{MR}}^T\left(\mathbf{H}_{\mathbf{x}\mathrm{MR}}(\mathrm{j}\omega)\mathbf{U}_{\mathrm{MR}}\mathbf{q}+\mathbf{H}_{\boldsymbol{\delta}\mathrm{MR}}(\mathrm{j}\omega)\boldsymbol{\delta}_{\mathrm{MR}}\right),\end{aligned} \tag{20}$$

which yields

$$\begin{aligned}\left(-\omega^2\mathbf{M}+\mathrm{j}\omega\mathbf{C}+\mathbf{K}-\mathbf{U}_{\mathrm{MR}}^T\mathbf{H}_{\mathbf{x}\mathrm{MR}}(\mathrm{j}\omega)\mathbf{U}_{\mathrm{MR}}\right)\mathbf{q} \\ = \mathbf{U}_{\mathrm{MR}}^T\mathbf{H}_{\boldsymbol{\delta}\mathrm{MR}}(\mathrm{j}\omega)\boldsymbol{\delta}_{\mathrm{MR}}\end{aligned} \tag{21}$$

As long as all the controls $\boldsymbol{\delta}$ are considered, including for example also the collective pitch of the tail rotor, i.e. $\boldsymbol{\delta} = \{\boldsymbol{\delta}_{\mathrm{MR}};\boldsymbol{\delta}_{\mathrm{TR}}\}$, the problem can be written as

$$\mathbf{q} = \mathbf{H}_{\mathbf{q}\boldsymbol{\delta}}(\mathrm{j}\omega)\boldsymbol{\delta}, \tag{22}$$

where additional exogenous inputs and disturbances are neglected, since the analysis focuses on coupled pilot-vehicle stability.

In order to account for the detailed pilot-vehicle interaction, actuator dynamics are considered as well. The dynamic relationship between the command requested by the pilot and the actual motion prescribed to the controls is

$$\boldsymbol{\delta} = \mathbf{H}_{\mathrm{act}}(\mathrm{j}\omega)\boldsymbol{\eta}+\mathbf{H}_{\mathrm{dc}}(\mathrm{j}\omega)\mathbf{f}_{\mathrm{act}}, \tag{23}$$

where vector $\boldsymbol{\eta}$ contains the motion of the control inceptors, while $\mathbf{f}_{\mathrm{act}}$ represents the force transmitted by the actuators; $\mathbf{H}_{\mathrm{dc}}(\mathrm{j}\omega)$, the dynamic compliance of the actuators, is usually neglected. Usually, a first- or second-order equation is considered for the actuator dynamics transfer function $\mathbf{H}_{\mathrm{act}}(\mathrm{j}\omega)$. The bandwidth of the actuators may have an impact on the interaction between the vehicle and the pilot mainly because it introduces a delay in the control.

3.3 Involuntary Pilot Model

The involuntary pilot model basically produces control inceptors motion as a function of the motion of the vehicle. In practice, the inceptor motion involuntarily produced by the pilot is often associated with the acceleration experienced by the pilot through the seat. The literature on the subject is scarce (see for example the work of Mayo on the involuntary collective motion associated with motion along the vertical axis, [22], and subsequent work by Masarati et al., [23], and the work by Parham et al. on the lateral axis, [24]). Analytical methods based on accurate biomechanical modeling of the pilot are being developed [25, 26], to support the determination of transfer function variability.

In general, a complete involuntary pilot model is expressed in the form

$$\boldsymbol{\eta} = \mathbf{H}_{\eta x}(\mathrm{j}\omega)\mathbf{x}_{\mathrm{pilot}}, \tag{24}$$

Table 2 Data for function $H_{\eta\ddot{z}_p}(s)$ based on Mayo's models [22]

	ectomorphic	**mesomorphic**
ω_p (radian/s)	21.267	23.567
ξ_p	0.322	0.282
τ_p (s)	0.118	0.108

where $\boldsymbol{\eta}$ are the involuntary contributions to the motion of the control inceptors, while $\mathbf{x}_{\mathrm{pilot}} = \mathbf{U}_{\mathrm{pilot}}\mathbf{q}$ is the motion of the seat.

In Mayo's work [22], the function expressed the absolute acceleration of the hand as a function of the absolute acceleration of the seat,

$$\begin{aligned}\ddot{z}_{\mathrm{hand}} &= H_{\ddot{z}_{\mathrm{hand}}\ddot{z}_{\mathrm{seat}}}\ddot{z}_{\mathrm{seat}} \\ &= \frac{sr_p/m_p+k_p/m_p}{s^2+s(r_p+r_c)/m_p+k_p/m_p}\ddot{z}_{\mathrm{seat}}\end{aligned} \tag{25}$$

The function can be reformulated in order to yield the collective input as a function of the acceleration of the seat by:

- transforming the absolute acceleration of the hand into its relative counterpart,

$$\ddot{z}_{\text{hand rel.}} = \ddot{z}_{\mathrm{hand}} - \ddot{z}_{\mathrm{seat}}; \tag{26}$$

- integrating the output twice,

$$z_{\text{hand rel.}} = \frac{1}{s^2}\ddot{z}_{\text{hand rel.}}; \tag{27}$$

- dividing the output by the length of the collective stick, namely

$$\eta = \frac{1}{L}z_{\text{hand rel.}}. \tag{28}$$

The resulting function is

$$\eta = -\frac{1}{sL}\frac{s+1/\tau_p}{s^2+2\xi_p\omega_p s+\omega_p^2}\ddot{z}_{\mathrm{seat}} \tag{29}$$

The values used in the modified form of Mayo's formula are reported in Table 2.

Similar functions can be formulated for the involuntary longitudinal and lateral cyclic controls resulting from surge (fore-aft motion) and sway (lateral motion) accelerations. When discussing numerical results, transfer functions and frequency response data from the literature are considered; since the original references did not provide analytical formulas, their interaction with the stability limits will be analyzed only graphically.

A complete description of the loop closure exerted by the pilot requires one to consider also the voluntary action. Since this contribution is band-limited at a crossover frequency of about $2\div3$ radian/s (the upper is a hard limit for typical human behavior, as discussed in [27]), it is not considered in the present work because its action is about one decade below typical biomechanical poles, which are in the

range 20÷25 radian/s, as shown in Table 2, and thus no significant interaction is expected with the aeroelasticity of rotorcraft. This implies that only results above 1 Hz must be considered.

3.4 Robust Analysis Problem

The robust stability analysis problem aims at determining the stability boundaries of the involuntary pilot model, considering the involuntary pilot as the uncertain element of an otherwise certain system.

The plant consists in the transfer matrix of the helicopter from the control inputs to the motion of the pilot seat. In principle, one may want to consider the nominal controls that are sent to the main and tail rotor in a conventional helicopter design,

$$\boldsymbol{\delta} = \left\{ \begin{array}{c} \boldsymbol{\delta}_{\mathrm{MR}} \\ \boldsymbol{\delta}_{\mathrm{TR}} \end{array} \right\} = \left\{ \begin{array}{c} \theta_{0\mathrm{MR}} \\ \theta_{1c\mathrm{MR}} \\ \theta_{1s\mathrm{MR}} \\ \theta_{0\mathrm{TR}} \end{array} \right\} \tag{30}$$

However, it may be more appropriate to decouple the uncertain pilot model from the kinematics and dynamics of the flight controls of a specific vehicle, thus considering as inputs the motion of the control inceptors,

$$\boldsymbol{\eta} = \left\{ \begin{array}{c} \eta_{\mathrm{collective}} \\ \eta_{\mathrm{longitudinal}} \\ \eta_{\mathrm{lateral}} \\ \eta_{\mathrm{pedal}} \end{array} \right\}. \tag{31}$$

In this latter case, any gearing ratio between the motion of the control inceptors, the actuator dynamics and the dynamics possibly associated with an Automatic Flight Control System (AFCS) in augmented helicopter designs can be included in the dynamic model of the vehicle.

As previously mentioned, the output of the plant consists of the motion of the pilot's seat,

$$\mathbf{x}_{\mathrm{pilot}} = \mathbf{U}_{\mathrm{pilot}}\mathbf{q}, \tag{32}$$

which, thanks to Eqs. (22) and (23), can be expressed as a function of the control inceptors,

$$\mathbf{x}_{\mathrm{pilot}} = \mathbf{U}_{\mathrm{pilot}}\mathbf{H}_{\mathbf{q\delta}}\mathbf{H}_{\mathrm{act}}\boldsymbol{\eta} = \mathbf{H}_{\mathbf{x}\eta}\boldsymbol{\eta}. \tag{33}$$

In general, thus, the motion of the seat is represented by a 6×1 vector, whereas the controls consist of a 4×1 vector. As a consequence, the reduced plant is represented by a 6×4 matrix, $\mathbf{G} = \mathbf{H}_{\mathbf{x}\eta}$. Consequently, the involuntary pilot model is represented by a 4×6 matrix, $\boldsymbol{\Delta} = -\mathbf{H}_{\boldsymbol{\eta x}}$. This implies that the coupled loop transfer matrix, $\mathbf{G}\boldsymbol{\Delta}$, is structurally rank deficient.

As discussed in [11], limit reference pilot models are represented by $\mathbf{H}_{\boldsymbol{\eta x}} \equiv \mathbf{0}$. In fact, when the pilot is absent, well balanced control inceptors do not usually move when the cockpit is subjected to accelerations. At the opposite extreme, an ideal, infinitely stiff pilot that firmly grasps the inceptors does not produce any involuntary input as a consequence of cockpit accelerations. For this reason, it is desirable to consider $\mathbf{H}_{\boldsymbol{\eta x}} = \mathbf{0}$ as the reference pilot. In this case, the reference coupled system is perfectly stable, since matrix $\mathbf{H}_{\mathrm{CL}} = \mathbf{I} + \mathbf{H}_{\boldsymbol{\eta x}}$ reduces to the identity, and its eigenvalues are well away from $(-1 + \mathrm{j}0)$.

The determination of robust stability consists in:

- determining the stability limits of the vehicle as indicated earlier;
- superimposing the transfer function of the pilot, taking into account any structure of its uncertainty;
- if the magnitude of the pilot transfer function does not exceed the magnitude of the vehicle limits, no instability can occur; otherwise,
- at crossings between the phase of the pilot transfer function and the vehicle limits, if the magnitude of the pilot transfer function exceeds that of the vehicle limits, an unstable condition is met.

This analysis is exemplified and clarified in the following section.

4 Numerical Results

The aeroelastic model discussed earlier has been used to determine the stability limits with respect to selected involuntary pilot inputs. Figures 5–7 contain the stability limits associated with the main rotor controls as functions of the motion of the pilot's seat in three directions. The limits associated with longitudinal cyclic caused by surge (fore-aft motion) of the seat are shown in Fig. 5. The limits associated with lateral cyclic caused by sway of the seat are shown in Fig. 6. The limits associated with collective caused by heave of the seat are shown in Fig. 7. Thick dashed lines represent the extreme values resulting from the three aeromechanics models; the thin dotted line represents the average value. The reader is warned that the dashed lines by no means enclose an envelope of possible boundaries; other models might result in further stability boundaries outside the areas surrounded by the dashed lines. Those lines merely define regions of plausible stability boundaries.

In all cases, the limits are computed using helicopter models that share the same airframe and controls dynamics, and differ in the aeroelasticity of the main rotor. In addition to the two models discussed earlier (blade element and BEM), a model derived from CAMRAD/JA is used as well. The stability limits resulting from the three models show relatively similar trends, especially in the band of frequencies of interest for the present analysis (1 Hz to 8 Hz), where the

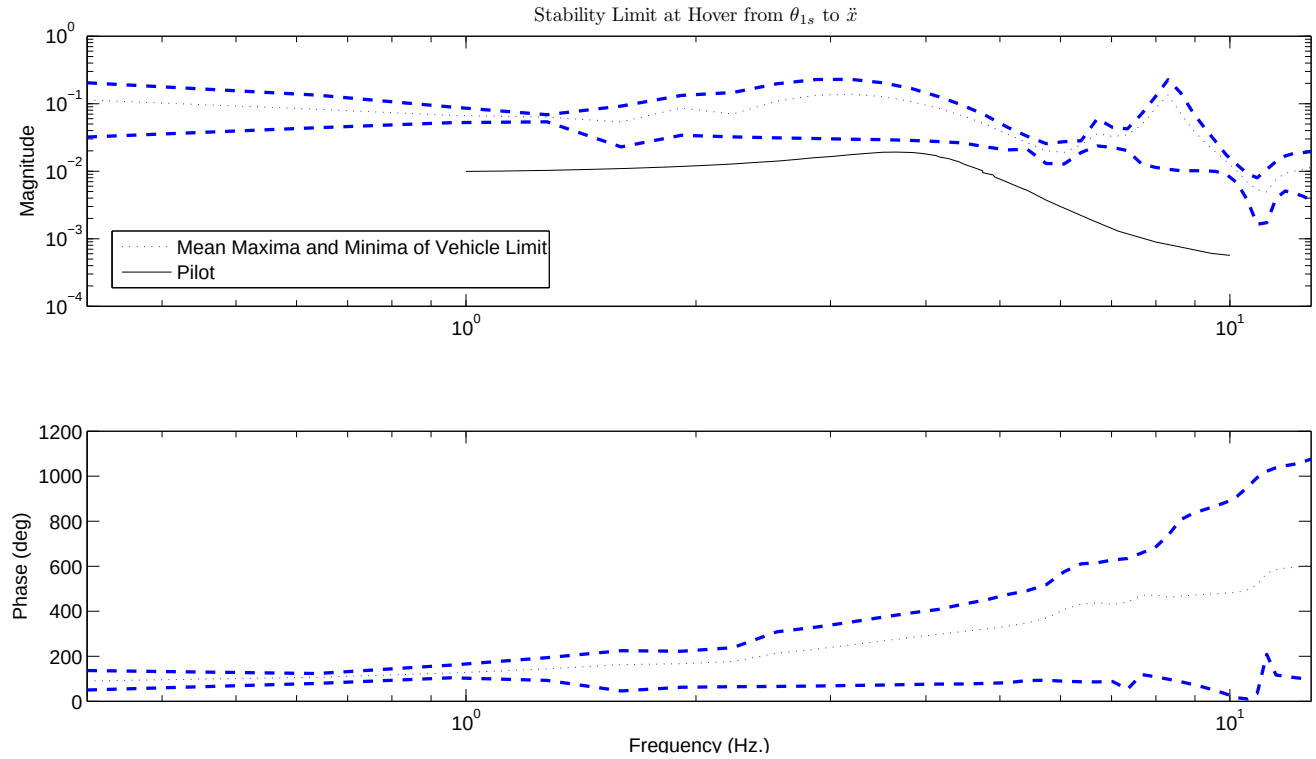

Fig. 5 Stability limits associated with longitudinal cyclic control induced by surge acceleration at the pilot's seat.

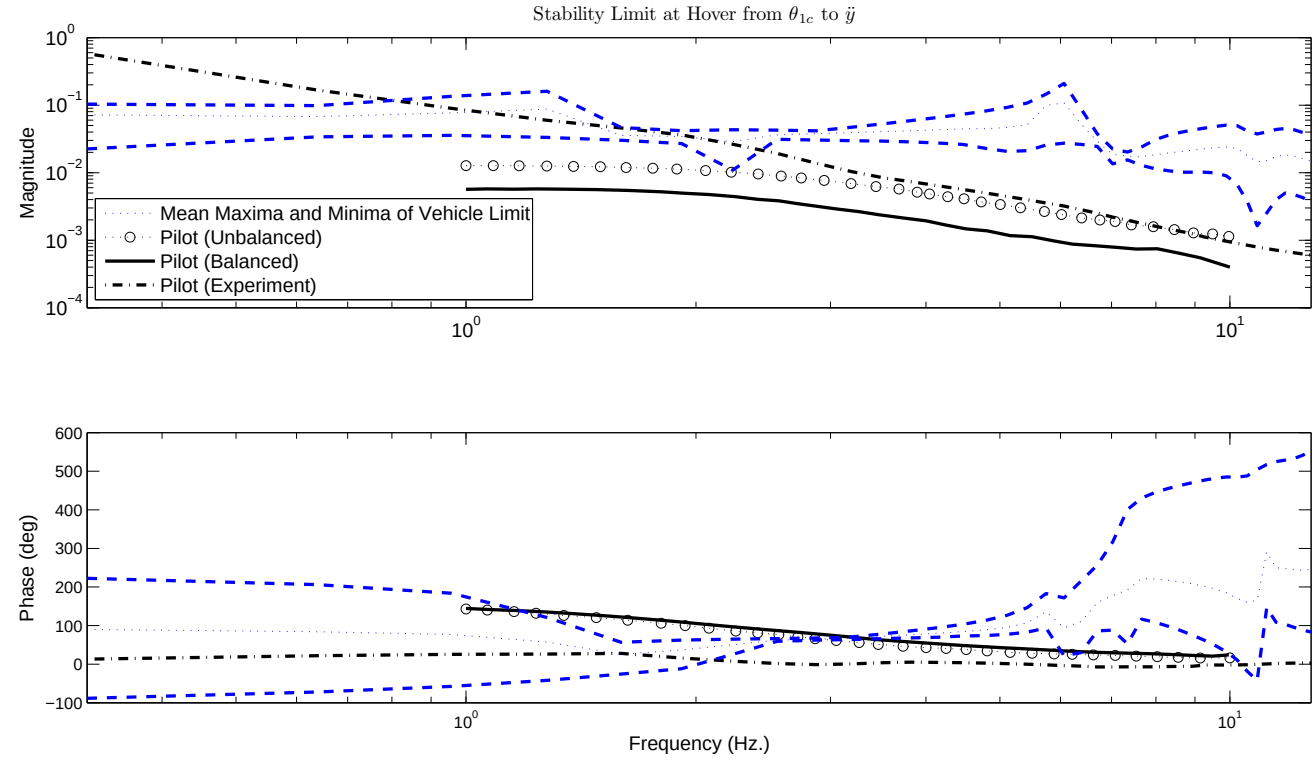

Fig. 6 Stability limits associated with lateral cyclic control induced by sway acceleration at the pilot's seat.

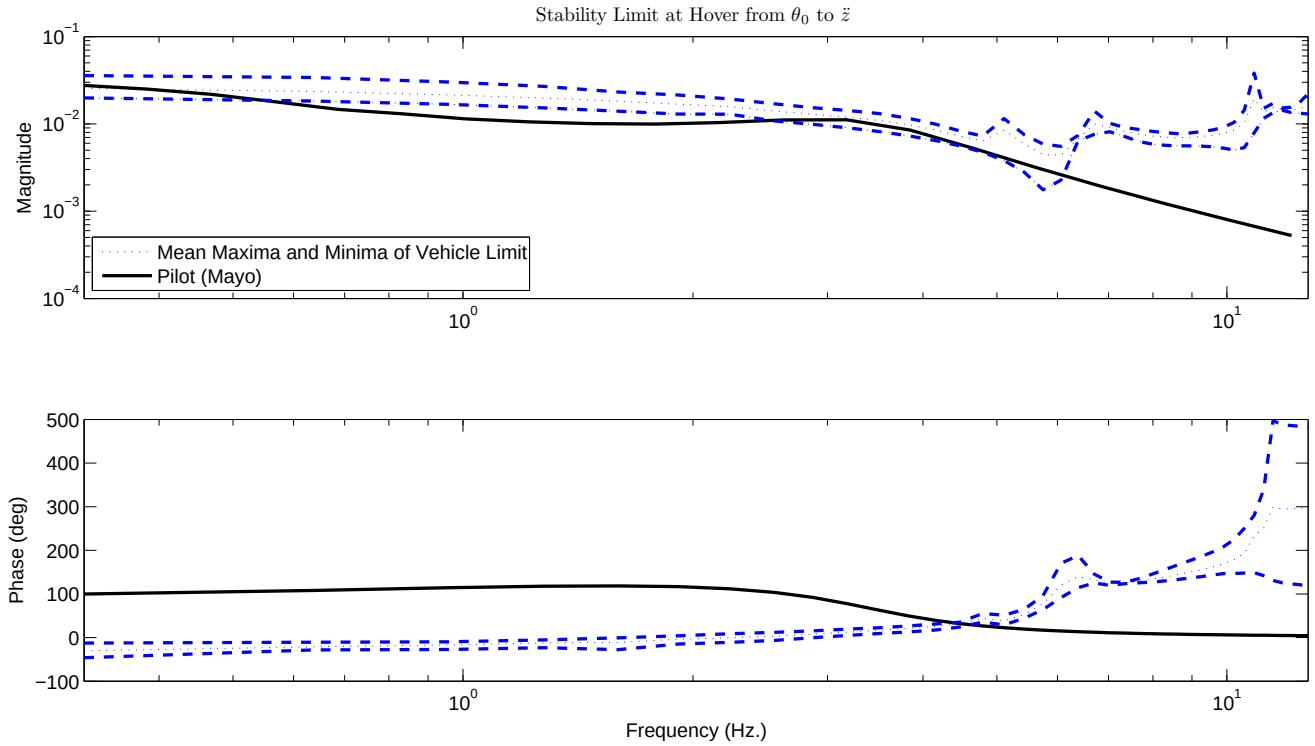

Fig. 7 Stability limits associated with collective control induced by heave acceleration at the pilot's seat.

analysis was refined. At lower and higher frequencies the limits differ, especially with respect to phase.

In order to illustrate the significance of the stability limits of the vehicle, they are compared with involuntary pilot models from the literature. In Fig. 5, the model of the involuntary longitudinal cyclic input caused by surge acceleration originally presented in Fig. 19 of Ref. [24] and related to the V-22 tiltrotor is considered. Unfortunately, no information about the phase was given in that reference. This function is used because the control device and the cockpit layout of the V-22 is similar to that of a conventional helicopter with respect to the needs of the present work.

In Fig. 6, the model of the involuntary lateral cyclic input caused by sway acceleration presented in Figs. 6 and 11 of Ref. [24] and again related to the V-22 is considered. In addition, experimental results obtained in the University of Liverpool's HELIFLIGHT flight simulator [23, 28] are considered.

Finally, in Fig. 7 the previously discussed model of the involuntary collective resulting from heave acceleration proposed by Mayo [22] is considered. The functions mentioned above do not specifically refer to the helicopter considered in the analysis; however, they are representative of pilot/control device arrangements that are common in helicopters. As such, they are presented to provide an indication of typical involuntary control transfer functions.

Figures 5–7 show that the stability boundaries resulting from the different aeromechanical models differ significantly in several regions of the frequency range considered in the plots. However, the differences tend to reduce and occasionally become negligible in the 2–5 Hz band, which contains most of the biomechanical models that may potentially adversely interact with the vehicle.

The graphical analysis shows that in the case of the surge motion of Fig. 5 no adverse interaction is possible, since the amplitude of the involuntary pilot control is always well below the limit.

On the contrary, in the case of the sway motion of Fig. 6 an instability can occur because the amplitude of some of the pilot models overcome some of the vehicle's limit curves, and this occurs when the phase of the related pilot curve is close to the phase associated with the critical direction of Eq. (16), illustrated in Fig. 2 as $e^{j\theta_i}$. Such potential instability is a consequence of the adverse interaction of the pilot's biomechanics with the main rotor regressive lead-lag mode, whose frequency is about 2 Hz and which is very lightly damped.

Similarly, in the case of the heave motion of Fig. 7, there is a slight chance of instability in the higher frequency portion of the frequency band, around 4.5 Hz, where the magnitude of the pilot's curve intersects the lower limit amplitude, since the phase of the pilot's curve approaches the phase associated with the critical direction. In this case, the potential

instability is a consequence of the adverse interaction of the pilot's biomechanical feedthrough with the main rotor coning mode.

It is worth recalling that the present analysis is essentially intended to illustrate the features of the proposed approach to robust stability analysis, and it does not imply any specific proneness of this helicopter model to adverse aeroelastic RPCs. Flight simulator testing of the proposed numerical models with respect to RPC is underway within ARISTOTEL to investigate adverse RPC and verify the predictions presented in this work.

5 Conclusions

A robust stability approach has been presented to study the proneness of helicopters to Rotorcraft-Pilot Couplings. The approach has been applied to the analysis of aeroelastic rotorcraft models of different complexity in the aerodynamics of the main rotor, from simple blade element theory to an original approach based on the Boundary Element Method. The interaction of the pilot biodynamic feedthrough with the dynamics of the vehicle has been discussed. Numerical results related to the comparison of stability limits of the different models have been discussed. All the aerodynamic models considered in the analysis show similar trends for the stability limits. The differences are limited especially in the frequency band of interest for the involuntary interaction with the pilot. Further investigation is needed to confirm this result and to determine whether it also applies to helicopters of different categories.

Acknowledgments

The research leading to these results has received funding from the European Community's Seventh Framework Programme (FP7/2007-2013) under grant agreement N. 266073.

References

1. Haniph A. Latchman, Oscar D. Crisalle, and V. R. Basker. The Nyquist robust stability margin — a new metric for the stability of uncertain systems. *International Journal of Robust and Nonlinear Control*, 7(2):211–226, February 1997. doi:10.1002/(SICI)1099-1239(199702)7:2<211::AID-RNC299>3.0.CO;2-8.
2. Sigurd Skogestad and Ian Postlethwaite. *Multivariable Feedback Control*. John Wiley & Sons, Chichester, 2005.
3. C. Döll, G. Ferreres, and J.-F. Magni. μ tools for flight control robustness assessment. *Aerospace Science and Technology*, 3(3):177–189, April 1999. doi:10.1016/S1270-9638(99)80041-8.
4. Francesco Amato, Raffaele Iervolino, Stefano Scala, and Leopoldo Verde. New criteria for the analysis of PIO based on robust stability methods. In *AIAA Atmospheric Flight Mechanics Conference*, Portland, OR, USA, August 9–11 1999. AIAA-1999-4006.
5. Francesco Amato, Raffaele Iervolino, Stefano Scala, and Leopoldo Verde. Category II pilot in-the-loop oscillations analysis from robust stability methods. *J. of Guidance, Control, and Dynamics*, 24(3):531–538, 2001. doi:10.2514/2.4743.
6. D. Borglund. Robust eigenvalue analysis using the structured singular value: The μ-p flutter method. *AIAA Journal*, 46(11):2806–2813, 2008. doi:10.2514/1.35859.
7. Martin Leijonhufvud and Anders Karlsson. Industrial application of robust aeroelastic analysis. *Journal of Aircraft*, 48(4):1176–1183, 2011. doi: 10.2514/1.55327.
8. Pierangelo Masarati, Vincenzo Muscarello, and Giuseppe Quaranta. Robust aeroservoelastic stability of helicopters: application to the air/ground resonance. In *American Helicopter Society 67th Annual Forum*, Virginia Beach, VA, May 3–5 2011.
9. Giuseppe Quaranta, Vincenzo Muscarello, and Pierangelo Masarati. Lead-lag damper robustness analysis for helicopter ground resonance. *J. of Guidance, Control, and Dynamics*, to be published. doi:10.2514/1.57188.
10. Vincenzo Muscarello, Pierangelo Masarati, and Giuseppe Quaranta. Robust aeroservoelastic analysis for the investigation of rotorcraft pilot couplings. In *3rd CEAS Air & Space Conference*, Venice, Italy, October 24–28 2011.
11. Giuseppe Quaranta, Pierangelo Masarati, and Joost Venrooij. Robust stability analysis: a tool to assess the impact of biodynamic feedthrough on rotorcraft. In *American Helicopter Society 68th Annual Forum*, Fort Worth, Texas, May 1–3 2012.
12. Pierangelo Masarati, Vincenzo Muscarello, and Giuseppe Quaranta. Linearized aeroservoelastic analysis of rotary-wing aircraft. In *36th European Rotorcraft Forum*, pages 099.1–10, Paris, France, September 7–9 2010.
13. Pierangelo Masarati, Vincenzo Muscarello, Giuseppe Quaranta, Alessandro Locatelli, Daniele Mangone, Luca Riviello, and Luca Viganò. An integrated environment for helicopter aeroservoelastic analysis: the ground resonance case. In *37th European Rotorcraft Forum*, pages 177.1–12, Gallarate, Italy, September 13–15 2011.
14. M. Gennaretti and G. Bernardini. Aeroacousto-elastic modeling for response analysis of helicopter rotors. In G. Buttazzo and A. Frediani, editors, *Variational Analysis and Aerospace Engineering: Mathematical Challenges for Aerospace Design*, pages 27–50. Springer Science+Business Media, LLC 2012, New York, 2012. doi:10.1007/978-1-4614-2435-2_2.
15. Massimo Gennaretti and Daniel Muro. Multiblade reduced-order aerodynamics for state-space aeroelastic modeling of rotors. *Journal of Aircraft*, 49(2):495–502, 2012. doi:10.2514/1.C031422.
16. Juan C. Cockburn and Blaise G. Morton. Linear fractional representations of uncertain systems. *Automatica*, 33(7):1263–1271, July 1997. doi:10.1016/S0005-1098(97)00049-6.
17. O. Dieterich, J. Götz, B. DangVu, H. Haverdings, P. Masarati, M. D. Pavel, M. Jump, and M. Gennaretti. Adverse rotorcraft-pilot coupling: Recent research activities in Europe. In *34th European Rotorcraft Forum*, Liverpool, UK, September 16–19 2008.
18. Gareth D. Padfield. *Helicopter Flight Dynamics: The Theory and Application of Flying Qualities and Simulation Modelling*. Blackwell Publishing, 2007.
19. D. H. Hodges and E. H. Dowell. Nonlinear equation for the elastic bending and torsion of twisted nonuniform rotor blades. TN D-7818, NASA, 1974.
20. M. Gennaretti and G. Bernardini. Novel boundary integral formulation for blade-vortex interaction aerodynamics of helicopter rotors. *AIAA Journal*, 45(6):1169–1176, 2007. doi:10.2514/1.18383.
21. S. Ianniello G. Bernardini, J. Serafini and M. Gennaretti. Assessment of computational models for the effect of aeroelasticity on BVI noise prediction. *Int'l J. of Aeroacoustics*, 6(3):199–222, 2007.

22. John R. Mayo. The involuntary participation of a human pilot in a helicopter collective control loop. In *15th European Rotorcraft Forum*, pages 81.1–12, Amsterdam, The Netherlands, 12–15 September 1989.
23. Pierangelo Masarati, Giuseppe Quaranta, and Michael Jump. Experimental and numerical helicopter pilot characterization for aeroelastic rotorcraft-pilot couplings analysis. *Proc. IMechE, Part G: J. Aerospace Engineering*, 227(1):124–140, January 2013. doi:10.1177/0954410011427662.
24. T. Parham, Jr., David Popelka, David G. Miller, and Arnold T. Froebel. V-22 pilot-in-the-loop aeroelastic stability analysis. In *American Helicopter Society 47th Annual Forum*, Phoenix, Arizona (USA), May 6–8 1991.
25. Andrea Zanoni, Pierangelo Masarati, and Giuseppe Quaranta. Upper limb mechanical impedance variability estimation by inverse dynamics and torque-less activation modes. In P. Eberhard and P. Ziegler, editors, *2nd Joint International Conference on Multibody System Dynamics*, Stuttgart, Germany, May 29–June 1 2012.
26. Pierangelo Masarati, Giuseppe Quaranta, and Andrea Zanoni. Dependence of helicopter pilots' biodynamic feedthrough on upper limbs' muscular activation patterns. *Proc. IMechE Part K: J. Multi-body Dynamics*, To be published.
27. Duane T. McRuer and Henry R. Jex. A review of quasi-linear pilot models. *Human Factors in Electronics, IEEE Transactions on*, HFE-8(3):231–249, September 1967. doi:10.1109/THFE.1967.234304.
28. M. Mattaboni, G. Quaranta, P. Masarati, and M. Jump. Experimental identification of rotorcraft pilots' biodynamic response for investigation of PAO events. In *35th European Rotorcraft Forum*, pages 1–12, Hamburg, Germany, September 22–25 2009.